

# Local Current Distribution and "Hot Spots" in the Integer Quantum Hall Regime

Yonatan Dubi<sup>1</sup>, Yigal Meir<sup>1,2</sup> and Yshai Avishai<sup>1,2,3</sup>

<sup>1</sup> *Physics Department, Ben-Gurion University, Beer Sheva 84105, Israel*

<sup>2</sup> *The Ilse Katz Center for Meso- and Nano-scale Science and Technology, Ben-Gurion University, Beer Sheva 84105, Israel*

<sup>3</sup> *Department of Applied Physics, University of Tokyo, Hongo Bunkyo-ku, Tokyo 113, Japan*

(Dated: August 10, 2018)

In a recent experiment, the local current distribution of a two-dimensional electron gas in the quantum Hall regime was probed by measuring the variation of the conductance due to local gating. The main experimental finding was the existence of "hot spots", i.e. regions with high degree of sensitivity to local gating, whose density increases as one approaches the quantum Hall transition. However, the direct connection between these "hot spots" and regions of high current flow is not clear. Here, based on a recent model for the quantum Hall transition consisting of a mixture of perfect and quantum links, the relation between the "hot spots" and the current distribution in the sample has been investigated. The model reproduces the observed dependence of the number and sizes of "hot spots" on the filling factor. It is further demonstrated that these "hot spots" are not located in regions where most of the current flows, but rather, in places where the currents flow both when injected from the left or from the right. A quantitative measure, the harmonic mean of these currents is introduced and correlates very well with the "hot spots" positions.

PACS numbers: 73.43.-f, 73.50.-h

## I. INTRODUCTION

The quantum Hall (QH) effect remains a major focus of interest,<sup>1</sup> despite the long time that has passed since its discovery. Apparently this is due to the ongoing technological progress employing new experimental probes and yielding new and sometimes surprising results. A particular issue, that has been under debate for quite some time, is related to the exact trajectories at which the current flows. Some theories suggest that the current flows mainly via edge states along the sample edges,<sup>3</sup> while others, based on the idea of a localization-delocalization transition at the centers of Landau levels, predict a distribution of currents extending throughout the bulk.<sup>4</sup> However, due to the robustness of the conductance quantization, the local properties are inaccessible via standard transport measurements. While some information on the current flow can be derived from static probes,<sup>5</sup> numerous attempts have been made to address these questions using various scanning imaging techniques,<sup>6</sup> commonly based on local probe of charge and electric potential. Yet, while proving successful in describing localized electronic states, these methods detect current only indirectly and cannot determine unambiguously how the current is partitioned between the edge and bulk channels.

Recently, a novel experimental approach has been applied to probe the local current distribution in a ballistic quantum point contact (QPC).<sup>7</sup> An atomic force microscope (AFM) tip was placed on top of the 2DEG in which a point contact was defined, causing a local depletion of electron density beneath it. The underlying assumption in this experiment is that this depletion strongly affects the conductance through the QPC only if the current density under the tip is high. On the other hand, the con-

ductance should not be modified if there is low current density under the tip. Thus, plotting the conductance change as a function of tip position results in an imaging of the electron current density. Indeed, the imaging clearly showed the different modes of the electronic wavefunction being successively occupied as the conductance through the QPC increases in quantized steps. Following this experiment a theoretical model was devised<sup>8</sup> which mimics this experiment and yields similar results for the distribution of current.

A similar experimental method has been used more recently to study the local current distribution in a 2DEG in the QH regime.<sup>9</sup> An AFM tip was placed on top of the Hall bar and locally gated the sample, thus changing the local potential beneath it. The resistance was then measured as a function of tip position and magnetic field. The main finding was that there are "hot spots" in the sample, i.e. isolated regions at which the conductance is extremely sensitive to the gating potential. These domains were interpreted as places where the current passes. They are mainly observed in the transition between plateaus, and disappear almost completely in the quantum Hall regime.

The fact that these measurement may not directly reflect the total current distribution in the sample can be understood through a simple example. Let us assume that there is a high barrier separating the left side and the right side of the sample. Then a current injected from either side (left or right) will be localized on that side of the barrier. Nevertheless, the only place where a change in the potential may induce a change in the conductance of the system is at the barrier itself, where no current actually flows. To put it in different terms, how can the measurement of the conductance, a quantity that

obeys specific Onsager relations with respect to reversing directions of the current and the magnetic field, yield information on the current distribution which, to the best of our knowledge, do not obey such symmetry relations?

Motivated by these experimentally relevant questions we employ in this work a recently proposed model for the QH transition<sup>14</sup> that enables a theoretical modelling of the experiment and allows for a detailed analysis of both the hot spots and of the spatial distribution of currents in the sample. Our main finding, beyond a good qualitative agreement with the experimental results, is that the hot spots are located at points where current passes both when it is injected from the left or from the right, and not necessarily at points where the current density is high. The number of such symmetry points is enhanced near the QH transition, but is small on either side of it, in agreement with the experimental results. We propose an empirical relation between the current distribution and the position of the "hot spots", based on a harmonic average of the current distributions when the current is injected from the left and from the right.

## II. MODEL

For the sake of completeness, let us briefly explain our model. In strong magnetic fields, electrons with Fermi energy  $\epsilon_F$  perform small oscillations around equipotential lines. When  $\epsilon_F$  is small, their trajectories are trapped inside potential valleys, with weak tunneling occurring between adjacent valleys. We associate each such potential valley with a site in a lattice. Nearest neighbor valleys (localized orbits) are connected by links representing quantum tunneling between them. As  $\epsilon_F$  increases and crosses the saddle point energy separating two neighboring valleys, the two isolated trajectories coalesce, the electron can freely move from one valley to its neighbor and the link connecting them becomes perfect. The QH transition occurs when an electron can traverse the sample along an equi-potential trajectory (an edge-state), which in the model corresponds to percolation of perfect links.

Consequently, the QH problem maps onto a mixture of perfect and quantum links on a lattice. Each link carries a left going and a right going channel. In accordance with the physics at strong magnetic fields there is no scattering in the junctions (valleys) and the edge state continues propagating uninterrupted according to its chirality (see Fig. 1(a)), while the scattering occurs on the link (saddle point) itself. Each scatterer is characterized by its scattering matrix  $S_i$ , namely a transmission probability  $T_i$  and phases. The phases are taken as random numbers from 0 to  $2\pi$  and the transmission amplitude of each link is determined by the height of the saddle point barrier between the neighboring valleys, taken from a uniform distribution  $U[-V, V]$ . The transmission is then determined locally by the local barrier height  $\epsilon$  and the Fermi

energy  $\epsilon_F$  by

$$T(\epsilon_F) = \exp[-\alpha(\epsilon - \epsilon_F)], \quad (1)$$

for  $\epsilon_F < \epsilon$ , where  $\alpha$  is some constant, and  $T(\epsilon_F) = 1$  for  $\epsilon_F > \epsilon$ . The transmission through the system,  $T$ , is then calculated using the scattering matrix approach and the conductance of the system is determined by the Landauer formula,  $G = \frac{2e^2}{h}T$ .

Within the scattering model, the current carried by the  $i$ -th link is given by  $J_i \propto |\psi_i^L|^2 - |\psi_o^L|^2$ , where  $\psi_{i(0)}^{L(R)}$  is the incoming (outgoing) wave function from the left (right) of the link (see Fig 2). Note that due to the unitarity of the S-matrix, the current is a locally left-right symmetric quantity, and is thus a property of the entire link.

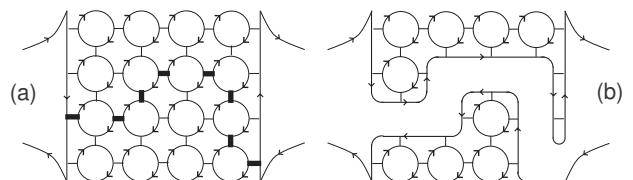


FIG. 1: Mapping of the problem onto a quantum percolation on a lattice: each link carries two counter propagating edge modes (a). A non zero transmission (thin lines) allows electrons to tunnel between adjacent sites (potential valleys). When the transmission is unity (bold lines in (a)), these two valleys merge, and an edge state can freely propagate from one to another. A percolation of these perfect transmission links (b) correspond to an edge state propagating through the system and a quantized conductance.

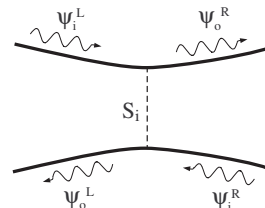


FIG. 2: Within the scattering model, each link is characterized by a scattering matrix  $S_i$ , connecting between the incoming and outgoing wave functions from left to right (see text).

As the Fermi energy increases, the conductance rises from zero to unity at the percolation threshold (Figs. 1(b) and 3). In Ref. 14 it was demonstrated that the phase transition described by the above model exhibits a critical exponent  $\nu \simeq 2.4$ , in agreement with numerical simulations for other models describing the QH transition. In this paper we simulate the experiment of Ref. 9 using the above model.

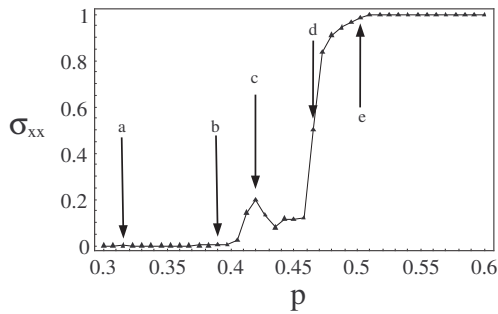


FIG. 3: Conductance as a function of probability  $p$ . The arrows point on the concentrations at which the current distribution (Fig. 4) and the hot spots (Fig. 10) are plotted.

### III. RESULTS

#### A. Current Distribution

In Fig. 3 the conductance (in units of  $2e^2/h$ ) of a  $20 \times 20$  size system<sup>15</sup> is plotted as a function of probability of a link to be perfect which corresponds to Fermi energy,  $p = \frac{81}{2} \left( \frac{\epsilon_F}{V} + 1 \right)$ . As can be seen, our model reproduces the conductance fluctuations close to the percolation transition<sup>10</sup>, which occurs (for this realization) at  $p = 0.505$ , close to the bulk classical percolation critical point.

The current distributions obtained for a specific realization of disorder for different values of  $p$  are depicted in Fig. 4 for two cases, when the current is injected from the left (left column) and from the right (right column), bright colors correspond to a high current. Each row corresponds a concentration  $p$  as denoted by arrows in Fig. 3. As can be seen, for low concentrations (i.e. on the insulating side of the transition, Fig. 3(a)-(b)) the currents flow in the system along some closed trajectory, returning back to the lead they came from due to the low transmission. In this realization the potential barrier separating left and right is located closer to the left side of the sample, thus an electron injected from the left is reflected almost immediately, while an electron injected from the right meanders through a larger part of the sample before being reflected.

Close to the transition the amount of current that passes through the system from one side to the other is roughly equal to the amount of back-scattered current, since the transmission of the system is close to  $T \approx 0.5$  (Fig. 3(c)-(d)). Here we find that the correlation between left- and right-originating current distributions is higher, and that the spatial distributions are broad, in accordance with percolation theory. Finally, for large concentrations (Fig. 3(e)) the transmission of the system is perfect, and thus the current passes between the leads following some trajectory, which corresponds to a percolating path of perfect links. As in the case of low concentration, the chirality causes strong separation be-

tween the distribution of left- and right-coming currents. A similar study, based on a tight-binding description,<sup>16</sup> have resulted with similar spatial current distributions, and has emphasized the role of the current chirality in the quantization of the Hall conductance and the vanishing of the longitudinal resistance far from the transition. The left-right a-symmetry in the presence of magnetic fields was also pointed out in Ref. 8.

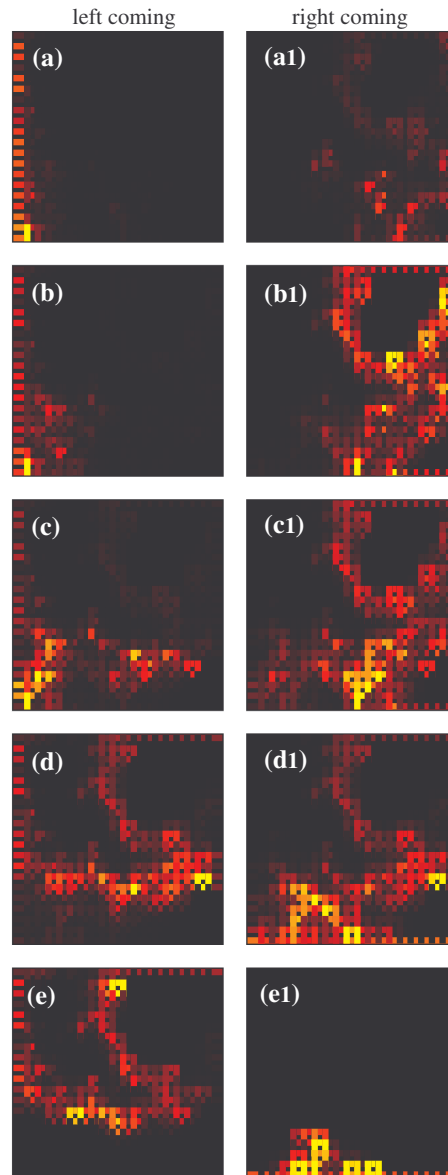


FIG. 4: Spatial current distribution when current is injected from the left (left column) or from the right (right column), for the concentrations depicted by arrows in Fig. 3. In the numeric calculation the current is injected from the upper-left-most or lower-right-most link, corresponding to left- or right-injected current. As seen, while far from the transition left- and right-coming currents are spatially separated, close to the transition the percolative nature of the system causes a wide spatial current distribution.

## B. Hot Spots

In order to simulate the "hot spots" experiment,<sup>9</sup> we mimic the local gating at a certain site by adding additional energy to the potential barriers surrounding that site, up to a distance of several lattice spacings. The conductance of the original lattice is then compared with that of the perturbed lattice for different values of the Fermi energy (corresponding to the experimental change in the magnetic field, or filling factor).

In Fig. 5 the spatial distribution of the change in the conductance is plotted for different values of  $p$ , corresponding to the points denoted  $b, c, d, e$  in Fig. 3. Brighter points correspond to the "hot spots" of the current, for which there is a sizable change in the conductance as that point in the lattice is gated by the AFM tip. The numerical data are normalized to the largest conductance change.

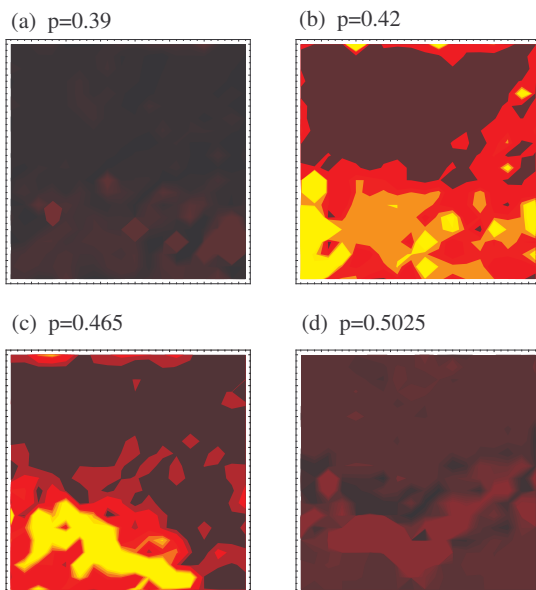


FIG. 5: Spatial mapping of the "hot spots" in the conductance, for probabilities corresponding to the arrows (b)-(e) in Fig. 3. Far below the QH transition (a) there are very few hot spots. Their number and intensity increases as one approaches the transition (b), is maximized at the transition region (c) and again diminishes above the transition (d).

As deduced from Fig. 5, both the amount and intensity (i.e. how considerable the influence of depleting sites from electrons on the conductance is) of the hot spots increase as one approaches the QH transition, in agreement with the experimental result. This may be seen more clearly by calculating the absolute value of the conductance change  $\delta\sigma$ , averaged over all the lattice sites and over disorder.  $\overline{\delta\sigma}$  is plotted in Fig. 6 for 100 disorder realizations. It is found that the maximal change in the conductance corresponds to the percolation thresh-

old, determined by the point at which the conductance is length-independent, denoted by an arrow in the inset of Fig. 6.

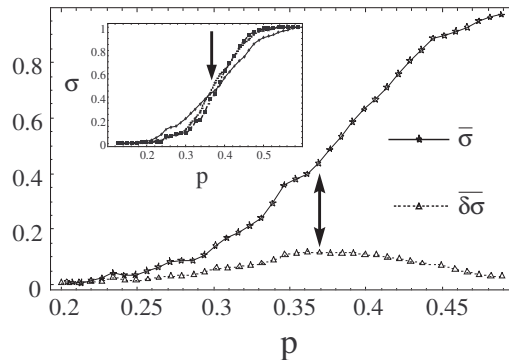


FIG. 6: Conductance (stars) and absolute value of the change in the conductance (triangles) as a function of concentration  $p$ , averaged over all lattice sites and over 100 realizations. The arrow indicates the point of percolation, defined as the point at which the disorder-average conductance is independent of system length. The inset shows the conductance for system lengths  $L = 10, 15, 20$ .

## C. Effect of tip parameters

Let us turn our attention to the role of the AFM tip. Experimentally, the exact effect of the AFM tip on the sample is unknown. However, it is reasonable to assume that the tip induces an increase in the potential energy in the area underneath it, which affects electrons up to a length  $l_{eff}$  away from it.

In order to address this point theoretically, we note that the tip has two main tunable parameters, namely the potential difference (voltage) between the tip and the sample,  $E_{tip}$ , and the distance between the tip and the sample. Changes in these experimental parameters affect two different aspects of the model: (a) a change in the offset of the energy in the links underneath the tip, namely the local potential energy change induced by the tip, and (b) a change in the effective length,  $l_{eff}$ , over which electrons feel the tip. While experimentally these two parameters are both affected, to some degree, by the tip height and voltage, theoretically one can study the change in each parameter separately. To simulate these effects, we repeat the above calculation, with a tip-induced exponential-enveloped change in the local potential barrier on the links,  $\Delta E = E_{tip}e^{-d/l_{eff}}$ , where  $d$  is the distance between the link and the position of the tip. In what follows we explore how changing either  $E_{tip}$  or  $l_{eff}$  affects the conductance change.

Changing  $E_{tip}$  does not have a significant effect on the spatial distribution of the hot spots, but only on their strength, namely the conductance change induced by the tip. In Fig. 7 we plot the average change in conductance  $\overline{\delta\sigma}$  (averaged over the entire sample) as a function of  $E_{tip}$ , varied from  $E_{tip} = 0$  to  $E_{tip} = V$ , that is of the order

of the band width. The calculation is performed for concentration  $p = 0.42125$ , where the number of hot spots is quite large, and  $l_{\text{eff}} = 1$  (in units of lattice spacing). As seen,  $\overline{\delta\sigma}$  increases monotonically with  $E_{\text{tip}}$ . In the inset of Fig. 7 we plot the conductance change  $\delta\sigma$  when the tip is over the strongest "hot spot" in the sample, and again, a monotonic increase in  $\delta\sigma$  is observed.

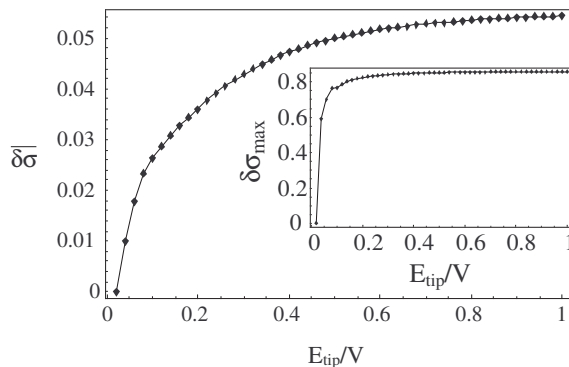


FIG. 7: Average change in conductance,  $\overline{\delta\sigma}$ , as a function of STM tip voltage  $E_{\text{tip}}$ , averaged over the entire sample. Inset : the same for the strongest "hot spot" in the sample.

Next we examine the effect of changing  $l_{\text{eff}}$ . One may naively guess that increasing  $l_{\text{eff}}$  should result in an increase in  $\delta\sigma$ . However, due to quantum interference this may not always be the case, especially far from the percolation transition, where the conductance change is rather small. In Fig. 8 We plot the spatial map of hot-spots for  $E_{\text{tip}} = V$  and  $p = 0.30875$  (which is close to the percolation transition for this sample, the sample having a transmission  $T = 0.648$  for this concentration), for  $l_{\text{eff}} = 1, 2, \dots, 8$  (in units of lattice constant). We find that although the number of hot-spots (indicated by bright colors) increases, their locations are changed, due to interference effects.

To make this more qualitative, in Fig. 9 we plot the average change in the conductance  $\overline{\delta\sigma}$ , averaged over the sample and over 100 realizations of disorder, for concentration  $p = 0.5$  (i.e. with Fermi energy at the center of the band), as a function of  $l_{\text{eff}}$ . We find that indeed, on average the conductance change exhibits a monotonic increase. However, for a given realization and a given tip position, changing  $l_{\text{eff}}$  (which corresponds to a change in the distance between tip and sample) may result in fluctuations in  $\delta\sigma$ , as plotted in the inset of Fig. 9.

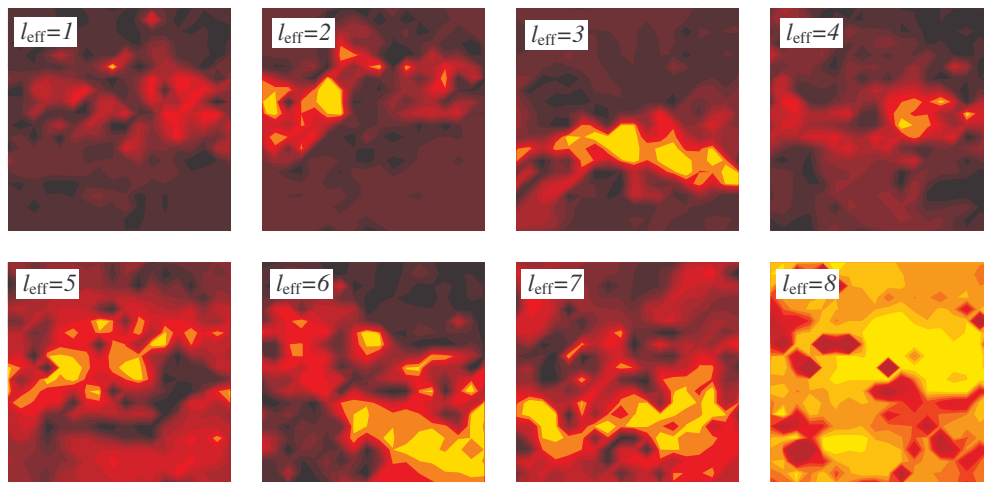


FIG. 8: Spatial map of hot-spots for different values of the STM tip effective length,  $l_{\text{eff}} = 1, 2, \dots, 8$ .

#### D. Relation Between Hot Spots and Current Distribution

Next, we ask the question: are the "hot spots" observed in experiment located at the extended, current

carrying electronic states in the bulk? As stated above, although one is inclined to give a positive answer, the different symmetry of the hot-spots and the current dis-

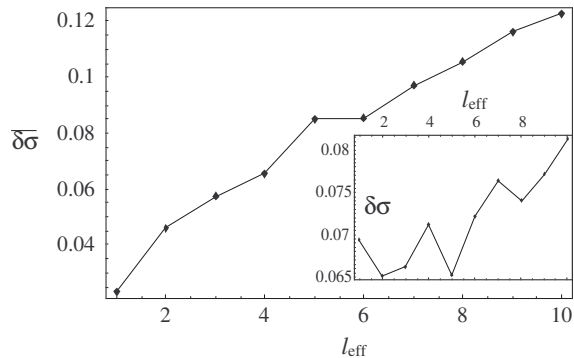


FIG. 9: Average conductance change,  $\overline{\delta\sigma}$ , averaged over the sample and over 100 realizations of disorder as a function of  $l_{\text{eff}}$ , showing a monotonic increase. Inset : the local change  $\delta\sigma$  at a given position and realization of disorder as a function of  $l_{\text{eff}}$ . One sees that  $\delta\sigma$  may fluctuate due to quantum interference.

tribution points that they cannot be identical. It is clear, however, that they are correlated, in a way we discuss below.

Let us examine the correlation between the hot-spots and current distribution<sup>17</sup>. Since the strength and location of the hot links is independent of the direction of the current injection, it is clear that the hot links are *not* located at the points where most of the current passes, as these depend sensitively on direction. Rather, it is found that the hot links are located at points which hold appreciable currents for both directions of current injection. To demonstrate this we plot on the left column of Fig. 10 the spatial image of a harmonic average of the local currents from the two directions of current injection. Bright spots thus correspond to links in which local current is significant in both directions of current injection. On the right column we plot the spatial image of the "hot links", that is, the conductance change due to setting the transmission on each link to zero. Both columns are shown for the concentrations corresponding to the arrows of Fig. 3. One clearly sees the correlation between the two images.

In order to make this correlation more quantitative the correlation function  $C(p)$  is defined to be the square of difference between the current and the conductance change, normalized and averaged over the entire sample. That is, let  $j_i$  be the normalized current in the  $i$ -th link (either when the current is injected from the left, from the right or a average of the two), and  $\delta\sigma_i$  be the normalized change in the conductance when the tip is placed over the  $i$ -th link (note that both  $j_i$  and  $\delta\sigma_i$  depend on the concentration  $p$ ), then  $C(p) = \frac{1}{N} \sum_i |j_i - \delta\sigma_i|^2$ . The smaller  $C(p)$  is, the higher is the correlation between these distributions. In Fig. 11  $C(p)$  is plotted for different concentrations  $p$ , when correlating between the hot links and the harmonic averaged current distribution (triangles), the hot-links and the left-coming (stars) and right-coming (squares) current distribution and between the hot-links and a random distribution (diamonds), that

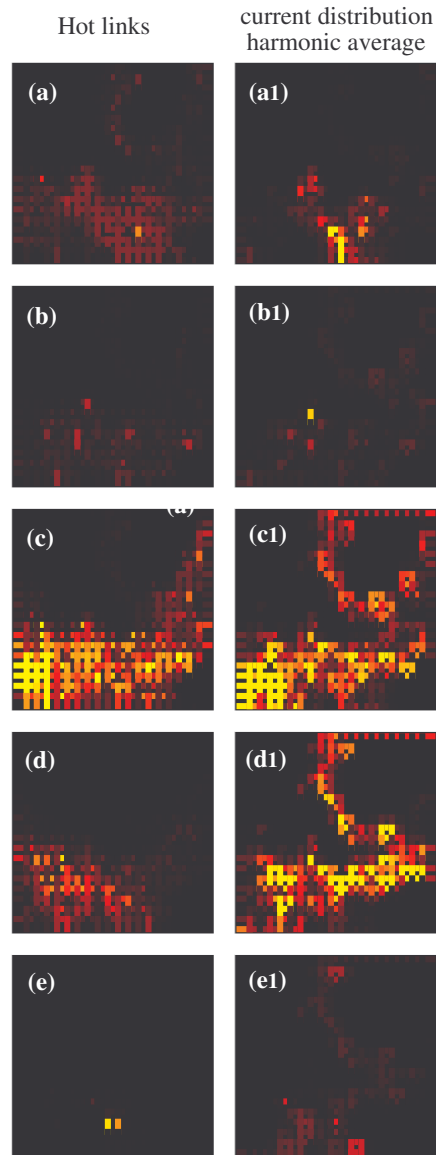


FIG. 10: Left column: a spatial image of the hot links, for the concentrations depicted by arrows in Fig. 3, bright links correspond to links with strong effect on the conductance. Right column: spatial image of the harmonic mean of local currents obtained from two different directions of voltage drop, for the same concentrations. Bright links correspond to links in which current is considerable for both directions of voltage drop. A clear correlation between the left and right columns is visible.

serves as a reference scale. As seen, the hot-links are well correlated with the harmonic-averaged current distribution, indicated by the low values of  $C(p)$ . The correlation between the hot-links and currents flowing from the left or from the right is much worse, and actually resembles the correlation with a completely random distribution for large concentrations.

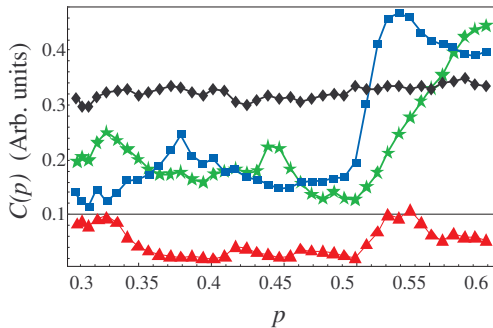


FIG. 11: Correlation function  $C(p)$  (see text), as a function of concentration. The correlation is between the hot-links and the harmonic-averaged current distribution (triangles), the hot-links and the left-coming (stars) and right-coming (squares) current distribution and between the hot-links and a random current distribution (diamonds). The lower the value of  $C(p)$ , the higher the correlation. The low value of the correlation function between the hot spots and the harmonic-average, relative to the other correlations, demonstrate that the hot spots do not directly reflect the total spatial current distribution, but only the transport current, estimated by the harmonic average.

#### IV. SUMMARY

In this work a recent model for the QH transition<sup>14</sup> have been used to shed light on an experiment in which a local AFM-tip induced local gating has been employed

to study the change in the resistance as a function of the tip location. The present theoretical study demonstrates the existence of "hot spots", regions with higher sensitivity to local gating. Our model, consisting of a coherent mixture of perfect and quantum links, qualitatively reproduces the experimental result. It was demonstrated that these "hot spots" do not lie in the current-carrying paths, but rather on areas in the sample where current flows both when it is injected from the left or from the right, that is on the left-right symmetric parts of the current carrying paths. Note that since the geometry employed in this study corresponds to a two-terminal geometry, the longitudinal conductance is trivially related to the Hall conductance, and thus one expect a similar behavior of the "hot spots" in the Hall conductance.

We conclude by noting that in order to verify our finding experimentally, one should imply a non-destructive local probing of the QH sample (that is, probing that does not affect the conductance), e.g. local current-induced magnetic field sensing, in addition to the above mentioned local AFM-tip gating, *on the same sample*. Such an experimental system may turn out to be useful for measuring local currents in other systems, such as disordered superconducting thin films, or Hall samples in the fractional QH regime.

We thank T. Ihn for valuable discussions. This research is partially supported by a grant from the Israeli Science Foundation (ISF).

<sup>1</sup> For a recent review see *The Quantum Hall Effect*, D. Yoshioka (Springer, New York, 2002).

<sup>2</sup> B. J. Van Wees, H. van Houten, C. W. J. Beenakker, J. G. Williamson, L. P. Kouwenhoven, D. van der Marel and C. T. Foxon, *Phys. Rev. Lett.* **60**, 848 (1988); D. A. Wharam, T. J. Thornton, R. Newbury, M. Pepper, H. Ahmed, J. E. F. Frost, D. G. Hasko, D. C. Peacock, D. A. Ritchie and G. A. C. Jones, *J. Phys. C:Solid State Phys.* **21**, L209 (1988).

<sup>3</sup> B. I. Halperin, *Phys. Rev. B* **25**, 2185 (1982); A. H. MacDonald, T. M. Rice and W. F. Brinkman, *Phys. Rev. B* **28**, 3648 (1983); M. Buttiker, *Phys. Rev. B* **38**, 9375 (1988); D. B. Chklovskii, B. I. Shklovskii and L. I. Glazman, *Phys. Rev. B* **46**, 4026 (1992).

<sup>4</sup> G. Diener and J. Collazo, *J. Phys. C* **21**, 305 (1988); H. Hirai and S. Komiyama, *Phys. Rev. B* **49**, 14012 (1994); K. Tsemekhman, V. Tsemekhman, C. Wexler and D. J. Thouless, *Solid State Commun.* **101**, 549 (1997).

<sup>5</sup> E. Yehel, A. Tsukernik, A. Palevski, and H. Shtrikman, *Phys. Rev. Lett.* **81**, 5201 (1998)

<sup>6</sup> S. H. Tessmer, P. I. Glicofridis, R. C. Ashoori, L. S. Levitov, M. R. Melloch, *Nature* **392**, 51 (1998); A. Yacoby, H.F. Hess, T.A. Fulton, L.N. Pfeiffer and K.W. West, *Solid State Communications* **111**, 1 (1999); G. Finkelstein, P. I. Glicofridis, R. C. Ashoori, and M. Shayegan, *Science* **289**, 90 (2000); K. L. McCormick, M. T. Woodside, M. Huang, M. Wu, P. L. McEuen, C. Duruoz and J. S. Harris, *Phys. Rev. B* **59**, 4654 (1999); N. B. Zhitenev, T. A. Fulton, A.

Yacoby, H. F. Hess, L. N. Pfeiffer and K. W. West, *Nature* **404**, 473 (2000);

<sup>7</sup> M. A. Topinka, B. J. LeRoy, S. E. J. Shaw, E. J. Heller, R. M. Westervelt, K. D. Maranowski, and A. C. Gossard, *Science* **29**, 289 (2000).

<sup>8</sup> G. Metalidis and P. Bruno, *Phys. Rev. B* **72**, 235304 (2005).

<sup>9</sup> A. Kicin, A. Pioda, T. Ihn, K. Ensslin, D. C. Driscoll, and A. C. Gossard *Phys. Rev. B* **70**, 205302 (2004).

<sup>10</sup> S. Cho and M. P. A. Fisher, *Phys. Rev. B* **55**, 1637 (1997).

<sup>11</sup> R. F. Kazarinov and S. Luryi, *Phys. Rev. B* **25**, 7626 (1982); S. A. Trugman, *Phys. Rev. B* **27**, 7539 (1983).

<sup>12</sup> for a review see, e.g., B.Huckestein, *Rev. Mod. Phys.* **67**, 357(1995).

<sup>13</sup> I.V.Kukushkin, V. I. Fal'ko, R. J. Haug, K. v. Klitzing and K. Eberl, *Phys. Rev. B* **53**,R13260 (1996); A. A. Shashkin, V. T. Dolgoplov, G. V. Kravchenko, M. Wendel, R. Schuster, J. P. Kotthaus, R. J. Haug, K. von Klitzing, K. Ploog, H. Nickel and W. Schlapp, *Phys. Rev. Lett.* **73**,3141 (1994).

<sup>14</sup> Y. Dubi, Y. Meir and Y. Avishai, *Phys. Rev. B* **71**,125311 (2005); Y. Dubi, Y. Meir and Y. Avishai, *Phys. Rev. Lett.* **94**,156406 (2005).

<sup>15</sup> The lattice was taken to be square. Since the QH transition is universal and geometry-independent we do not expect the lattice shape to affect the results.

<sup>16</sup> A. Cresti, G. Grosso and G. P. Parravicini, *Phys. Rev. B*

**69**, 233313 (2004).

<sup>17</sup> In order to be able to compare links in the model, the calculation described in Sec. III B was repeated with the minor change that instead of raising the energy of several

barriers around a certain lattice site, we now calculate the change in conductance due to cutting each link. This way the "hot links" were mapped, which may be compared to the distribution of currents.